UNCERTAINTY PROJECTED MAPPING WITH APPLICATION TO REGIONAL SEISMIC HAZARD ANALYSIS

H. Goto[(1)], A. Chakraborty[(2)]

[(1)] *Associate Professor, Disaster Prevention Research Institute, Kyoto University, goto@catfish.dpri.kyoto-u.ac.jp*
[(2)] *Graduate Student, Graduate School of Engineering, Kyoto University, anirban@catfish.dpri.kyoto-u.ac.jp*

Abstract

In recent decades, various scales of seismic hazard have been analyzed. One typical output is the seismic hazard map that draws a spatial distribution of the hazard potentials for the sake of emphasizing the spatial differences. However, the map often causes a bias that people living in low potential area do not take any actions for disaster reduction. We suppose that the reason is uncertainty involved in mapped spatial data as well as the cognitive bias. Chakraborty and Goto (2018) proposed to vary map resolution with degree of the data uncertainty, namely Uncertainty Projected Mapping (UPM). Here, we introduce the principal concept of UPM, and several applications to regional seismic hazard analysis. In one example, nonlinear site amplifications in Osaka area are numerically simulated with a variety of input waves. The simulated samples of amplification factor, i.e. PGA amplification, are projected on the spatial map using the UPM. The map clearly shows where to highlight the amplification in terms of statistical significance.

Keywords: Seismic Hazard Map; Uncertainty Projected Mapping; Site Amplification; Bayesian Inference

1. Introduction

In recent decades, various scales of seismic hazard have been analyzed. One typical output is the seismic hazard map that draws a spatial distribution of the hazard potentials for the sake of emphasizing the spatial difference; i.e. landslide potentials, inundation area due to flood and/or tsunami, expected ground motion over decades, etc. However, the map often causes a bias that people living in low potential area do not take any actions for disaster reduction. This means that the hazard map may not only contribute to the disaster mitigation, but may also enhance the disaster.

We suppose that the reason is uncertainty involved in mapped spatial data as well as the cognitive bias. A smoother image or an image composed of large bins (pixels) are preferred if the hazard data contains less information. It means that the amount of information controls the resolution of images. However, the data uncertainty, which means amount of containing information, is not always spatially uniform.

Chakraborty and Goto [1] proposed to vary map resolution with degree of the data uncertainty, namely uncertainty projected mapping (UPM). As shown in Fig.1, UPM aims to draw a map so that a sharp color transition reflects a low uncertainty, and smooth transition reflects high uncertainty. UPM can show both the model and its uncertainty in a single plot.

In this article, we introduce the principal concept of UPM, and several applications to regional seismic hazard analysis. In one example, nonlinear site amplifications in Osaka area are numerically simulated with a variety of input waves. The simulated samples of amplification factor, i.e. PGA amplification, are projected on the spatial map using the UPM. The map clearly shows where to highlight the amplification in terms of statistical significance.

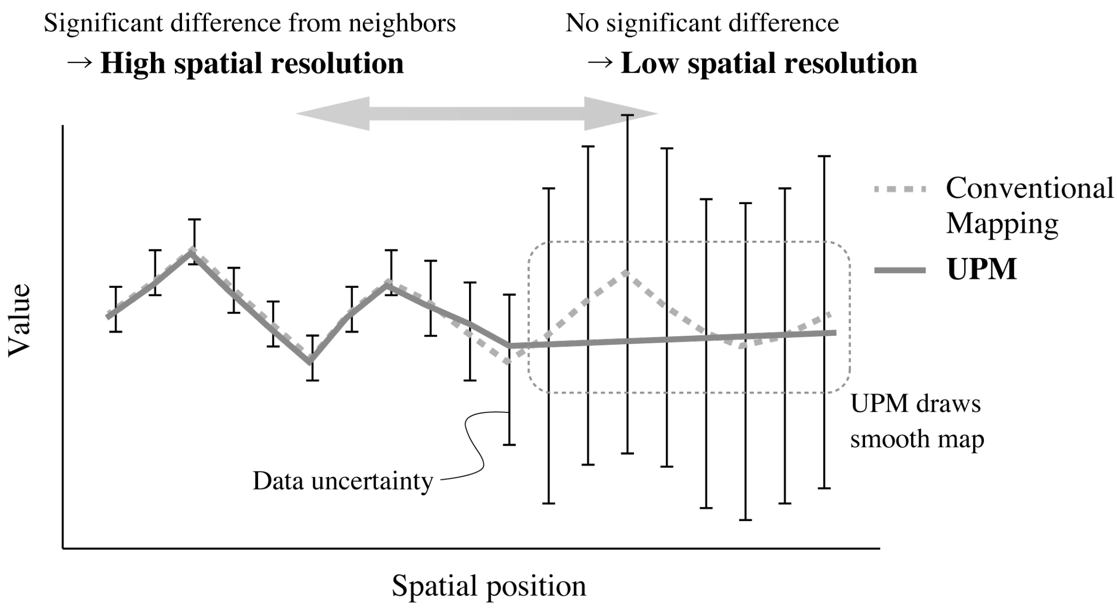

Fig. 1 – Principal concept of UPM

2. Uncertainty Projected Mapping (UPM)

Uncertainty projected mapping (UPM) [1] assumes the mapped variable to be a stochastic variable Y_l at spatial location l. Observation data y_{il} ($i = 1, \cdots, n_l$) is a set of samples from the stochastic variable, which obeys the following hierarchal Bayesian model.

$$Y_l \sim N(\mu_l, \sigma_l^2) \tag{1}$$

$$\mu_l \sim N\left(\sum_j w_{lj}\mu_j, s_l^2\right) \tag{2}$$

$$c = \sigma_l \, s_l \tag{3}$$

where μ_l, σ_l are model parameters that describe normal stochastic variable Y_l. Eq.(2) represents intrinsic conditional autoregressive model (CAR) [2,3,4] that can introduce the spatial structure of μ_l. w_{lj} is a normalized adjacency matrix ($\Sigma_j\, w_{lj} = 1$), whose all diagonal terms are zero ($w_{ll} = 0$). s_l is another model parameter that controls a spatial variation; i.e. smaller value of s_l provides smoother μ_l distribution. Chakraborty and Goto [1] proposed Eq.(3) that constrains the observation variance and the spatial variation. This aims to resolve fine images in an area with small sample variations in contrast to the large variations. c is a hyperparameter of the hierarchal Bayesian model.

Posterior probability of model parameters is analyzed on the basis of Bayes' theorem.

$$p(\mu_l, \sigma_l | \, y_{il}) \propto p(y_{il} | \, \mu_l, \sigma_l)\, p\left(\mu_l \middle| \sum_j w_{lj}\mu_l, s_l\right) \tag{4}$$

The right hand side are likelihood function and probability density function defined from Eqs.(1) and (2), respectively. Original UPM [1] evaluates both the posterior probabilities μ_l and σ_l, which are numerically simulated from Markov chain Monte Carlo (MCMC) [5,6,7], and plots expectation value of the marginal posterior probability, $E[p(\mu_l | \, y_{il})]$.

Model hyperparameter c controls the total smoothness of the spatial distribution. The value is selected from the balance between a goodness of fit and a prediction error in a framework of information criterion. Akaike's Bayesian Information Criterion (ABIC) (Akaike, 1980) has been widely adopted in the model selection. Recently, more general criteria have been proposed, namely widely applicable information criterion (WAIC) (Watanabe, 2009; Watanabe, 2010), and widely applicable Bayesian information criterion (WBIC) (Watanabe, 2013), whose computations are much compatible with MCMC simulation. The former WAIC is suitable for data prediction, and the latter WBIC is for model selection. In this study, we adopt WAIC in selecting c because the hazard maps aim to predict the values.

3. Application – Nonlinear site amplifications in Osaka area

Site amplification during strong earthquakes varies highly depending on the input waves because of nonlinearity of the soil deposit. If an earthquake scenario at the target area is unconditionally accepted, the scenario waves are allowed to be input motions, and the results are simply evaluated. However, in reality, various types of earthquakes can occur. It is important to evaluate the map of site amplification in considering the input wave sensitivity. We then comprehensively input records from all the available ones obtained in Japan, and use this variation in plotting a site amplification map in Osaka area.

3.1 Input motions

From the past studies in Osaka area, a stiff sand layer, namely Dg2, is selected as the engineering basement excepting the area of Uemachi plateau and the bay area. Since the Dg2 is approximately 400m/s of S-wave velocity, we select the K-NET and KiK-net stations on stiff soil with about 400m/s of S-wave velocity that is defined in a range of 400-700m/s of the average S-wave velocities up to 5m depth (Vs5). The selected stations are 60 for K-NET and 70 for KiK-net.

We select records obtained at these stations with a seismic intensity in JMA scale of 4.5 to 5.0. Finally, 14 records from K-NET and 12 records from KiK-net are selected. Although the records satisfy a criteria, aftershocks immediately after the main shock of the 2011 Tohoku earthquake are eliminated because the long coda of the main shock was included in these records. Fig.2 shows the histogram of PGA and acceleration response spectrum (Sa; h=0.05) in horizontal components of the 26 selected records. PGA is mostly distributed in a range of 100-500cm/s^2, and two exceptional records exceeding 600cm/s^2. Acceleration response is close to the value of PGA up to 0.5s, and gradually decreases in the similar slopes.

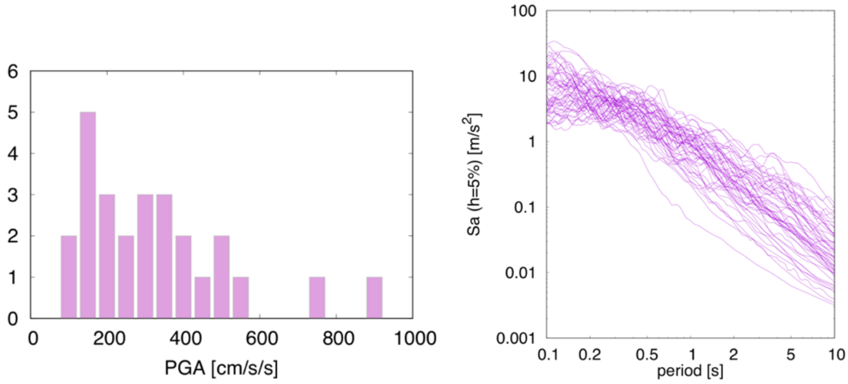

Fig. 2 – Histograms of PGA (left) and Sa (right) of the 26 selected records.

3.2 Simulating nonlinear response

Nonlinear site response for the 26 input waves is simulated using surface soil model in Osaka area evaluated in each 250m area. 1560 meshes, where the model up to the Dg2 layer has been modeled, are the selected in this study (Fig.3). The meshes almost cover the center of Osaka area excepting the Uemachi plateau and the bay area. Each model consists of layers classifying soil types, ages, density, N values, and estimated S-wave velocity in every 1m depth. As following the past study [12], the soil layers are classified into Ma13, Dg1, and Ma12 layers, and the representative H-D model studied in the laboratory experiments in this area is given as the nonlinear models. A half-space engineering basement with 400m/s of S-wave velocity is assumed at the bottom of the models.

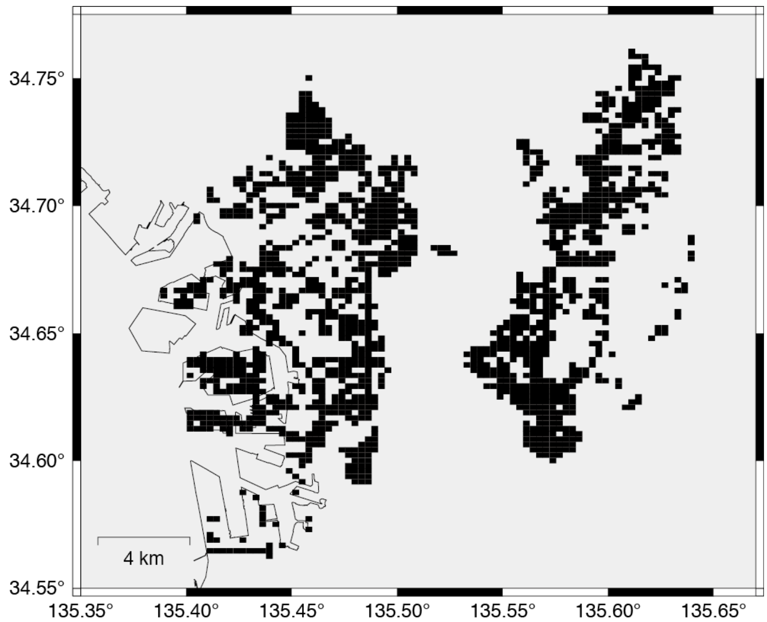

Fig. 3 – Target meshes (solid square) simulating the nonlinear site responses.

The 26 selected waves are simultaneously input to each two horizontal components. The nonlinear response is evaluated from equivalent linear analysis using SHAKE. We study 4 site factors; (1) amplification of maximum acceleration (PGA), (2) amplification of maximum velocity (PGV), (3) average of transfer function in 1.0-2.0Hz (F12), and (4) average of transfer function in 2.0-4.0Hz (F24). Fig.4 shows the average value over the simulated results from the 26 input waves obtained at each target mesh. Different spatial patterns are shown for each site factor, whereas the variation is particularly large in the PGA amplification. However, this spatial distribution shows only the average values. The large spatial variation does not mean large uncertainty. Fig.4 also shows the simulated variations along an east-west profile. Each sample corresponds to each result from the 26 input motions. Site factors of F12 and F24 are the smaller variations than the PGA and PGV ones. It suggests the map for F12 and F24 must be well resolved in this mesh scales. On the other hand, the PGA and PGV amplifications may not be discussed well in statistical point of view.

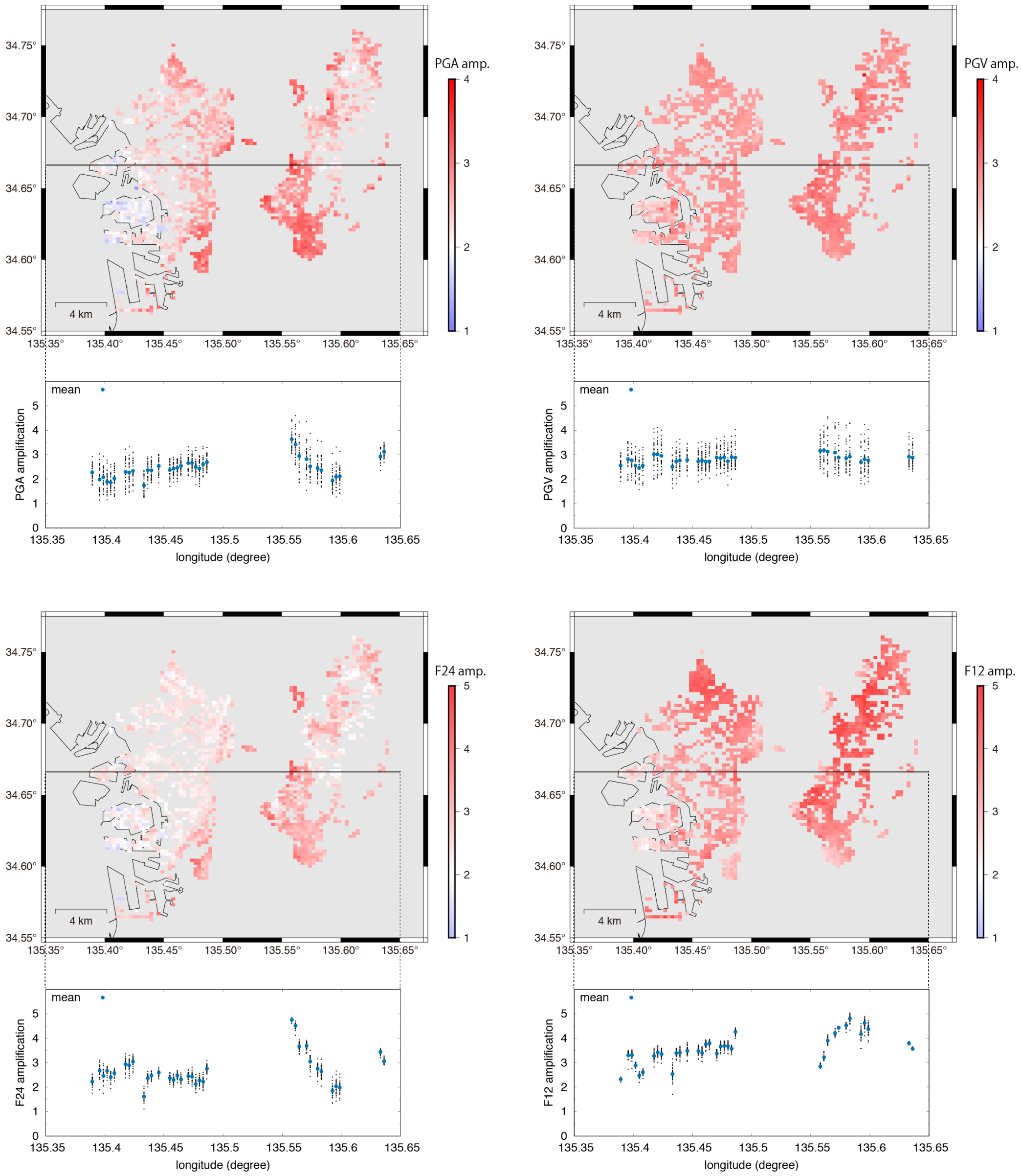

Fig. 4 – Average and variation of the simulated site factors.
(top left: PGA, top right: PGV, bottom left: F24, bottom right F12)

3.3 UPM of nonlinear site amplification

We apply UPM to the simulated samples of nonlinear site response. The adjacency matrix is established so that adjacent mesh structure can be introduced. The hyperparameter c is searched to minimize the WAIC. Fig.5 shows an example of map given different values of c. The smaller c value results smoother spatial distribution than the simple mean of samples, whereas it almost converges to the simple means as increasing the c value.

Fig.6 shows distribution of each site factor evaluated from UPM. Each panel shows amplification factor of PGA, PGV, F12, and F24, respectively. The spatial images by UPM are relatively smooth comparable to the simple mean (Fig.4), especially for PGA and PGV. This reflects the sample variation, as shown in Fig.4.

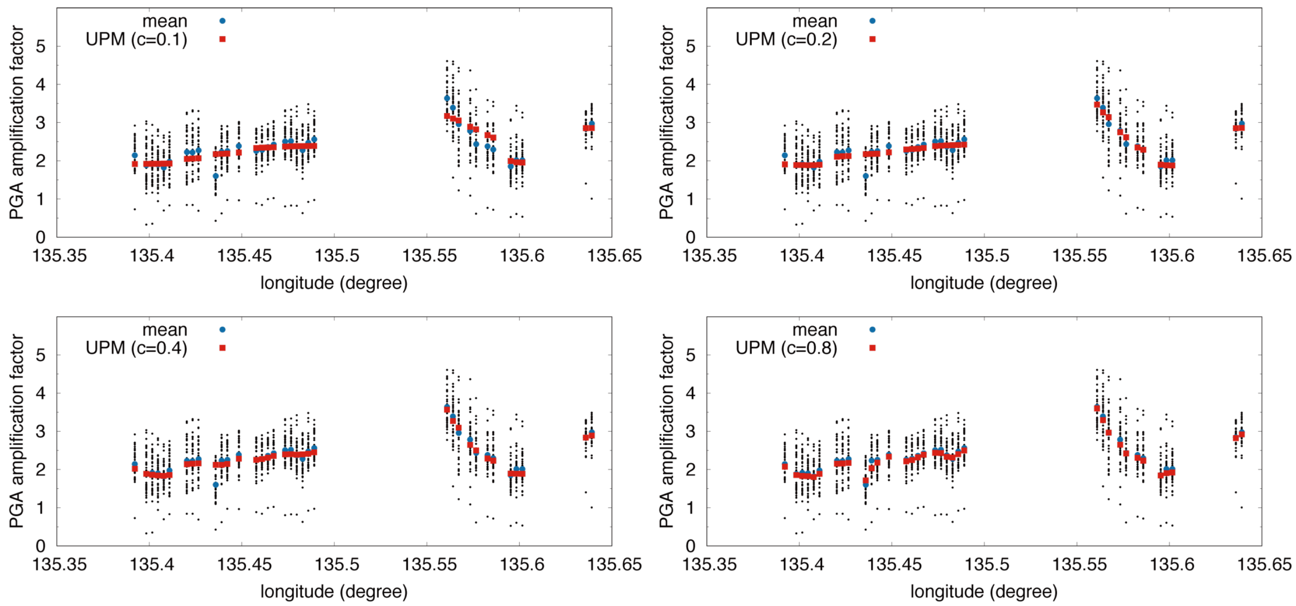

Fig. 5 – Effect of the hyperparameter c in UPM solution.

4. Discussion and conclusion

In this article, we explain some of the details of UPM and show an application to nonlinear site amplification in Osaka area. The evaluated map shows relatively smooth image by reflecting the sample variations. The map guarantees image resolution that a sharp color transition means a low uncertainty, and smooth transition means high uncertainty. This can avoid for human to underestimate the hazard potential in case of the lack of information.

Notice that results in this article represent only the amplification from the engineering basement. Actual ground motion in Osaka area is amplified by the 3D deep basin structure. The lower frequency components and some related index, e.g. PGV will be underestimated in this analysis. In this article, we aim to demonstrate the effectiveness of UPM in simulating the nonlinear site amplification, and it can be utilized to the precise analysis in considering the deep basin structures.

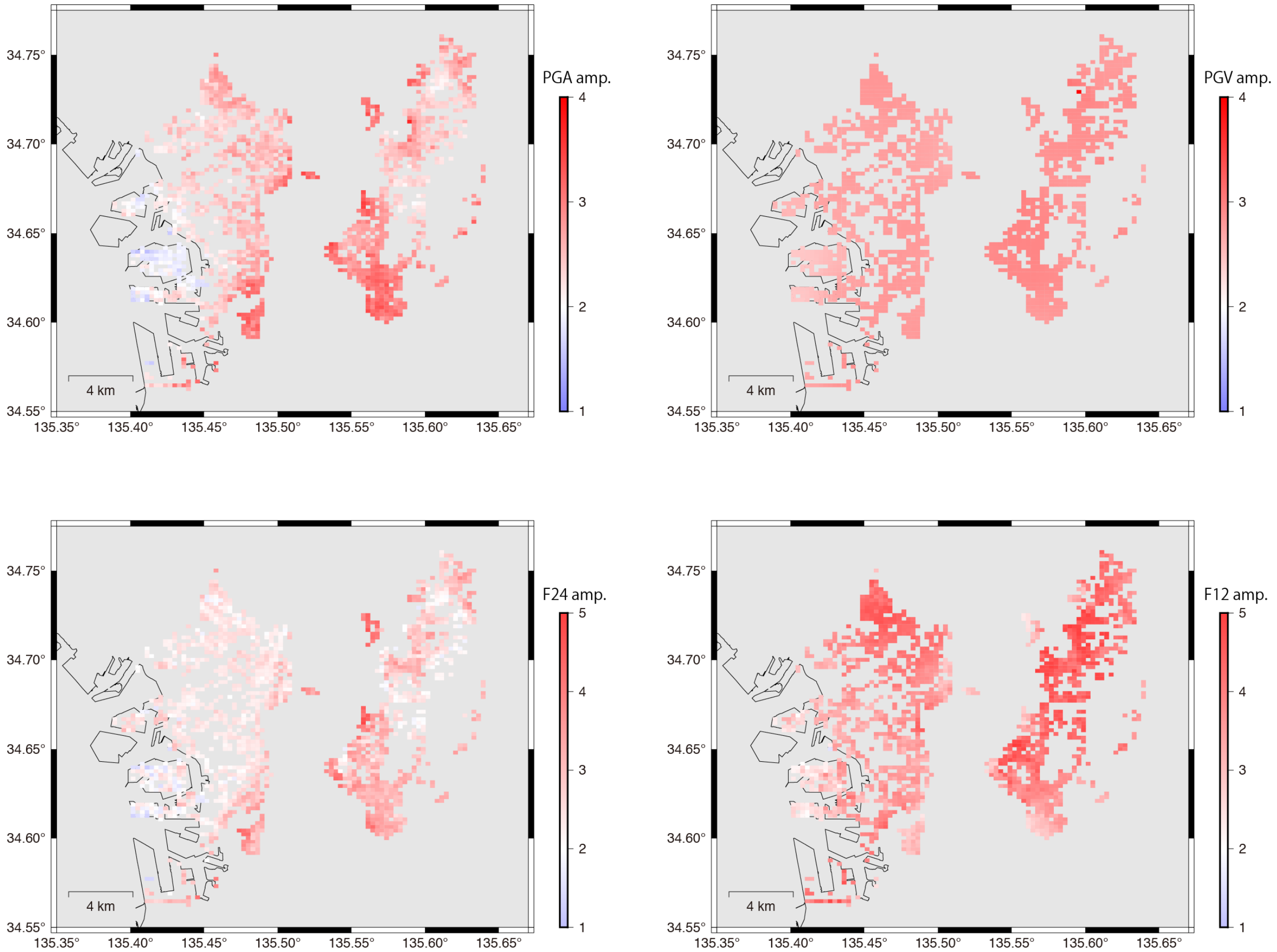

Fig. 6 – UPM of each site factor.
(top left: PGA, top right: PGV, bottom left: F24, bottom right F12)

5. Acknowledgements

Strong motion records are provided by National Research Institute for Earth Science and Disaster Resilience (K-NET and KiK-neth; http://www.kyoshin.bosai.go.jp). This work was supported by KAKENHI, Japan Society for the Promotion of Science (19H02400 and 19H02224).

6. References

[1] Chakraborty A, Goto H (2018): A Bayesian model reflecting uncertainties on map resolutions with application to the study of site response variation, *Geophys. J. Int.* **214**(3), 2264-2276.

[2] Besag J (1974): Spatial interaction and the statistical analysis of lattice systems, *J. R. Stat. Soc. Ser. B*, **36**(2), 192-236.

[3] Besag J, Kooperberg C (1995): On conditional and intrinsic autoregression, *Biometrika*, **82**(4), 733-746.

[4] De Oliveira V (2012): Bayesian analysis of conditional autoregressive models, *Ann. Inst. Stat. Math*, **64**, 107-133.

[5] Hastings WK (1970): Monte Carlo sampling methods using Markov chains and their applications, *Biometrika*, **57**(1), 97-109.

[6] Geman S, Geman D (1984): Stochastic relaxation, Gibbs distributions, and the Bayesian restoration of images, *IEEE Trans. Pattern Anal. Mach. Intell.*, **6**(6), 721-741.

[7] Goodman A, Weare J (2010): Ensemble samplers with affine invariance, *Comm. App. Math and Comp. Sci.*, **5**(1), 65-80.

[8] Akaike H (1980): Likelihood and the Bayes procedure, *Trabajos de Estadistica Y de Investigacion Operativa*, **31**(1), 143-166.

[9] Watanabe S (2009): Equations of states in singular statistical estimation, *Neural Networks*, **23**(1), 20-34.

[10] Watanabe S (2010): Asymptotic equivalence of Bayes cross validation and widely applicable information criterion in singular learning theory, *J. Mach. Learn. Res.*, **11**, 3571-3594.

[11] Watanabe S (2013): A widely applicable Bayesian information criterion, *J. Mach. Learn. Res.*, **14**, 867-897.

[12] Goto H, Hamada A, Nakamura Y, Oshima A, Kai S, Kageyama K, Kasugai M, Sagawa A, Tsutsumi A, Nagai H, Bando S, Fukai H (2018): Effect of nonlinear soil model on nonlinear site response analysis -application in Osaka area-, *Proc. Kansai Geo-Symposium 2018*. (in Japanese)

